Estimating asymptotic phase and amplitude functions of limit-cycle oscillators from time series data

Norihisa Namura *
Department of Systems and Control Engineering, Tokyo Institute of Technology, Tokyo 152-8552, Japan

Shohei Takata
Department of Systems and Control Engineering, Tokyo Institute of Technology, Tokyo 152-8552, Japan

Katsunori Yamaguchi
Department of Systems and Control Engineering, Tokyo Institute of Technology, Tokyo 152-8552, Japan

Ryota Kobayashi
Graduate School of Frontier Sciences, The University of Tokyo, Chiba 277-8561, Japan;
Mathematics and Informatics Center, The University of Tokyo, Tokyo 113-8656, Japan;
and JST, PRESTO, Saitama 332-0012, Japan

Hiroya Nakao
Department of Systems and Control Engineering, Tokyo Institute of Technology, Tokyo 152-8552, Japan

(Received 3 March 2022; accepted 13 June 2022; published 7 July 2022)

We propose a method for estimating the asymptotic phase and amplitude functions of limit-cycle oscillators using observed time series data without prior knowledge of their dynamical equations. The estimation is performed by polynomial regression and can be solved as a convex optimization problem. The validity of the proposed method is numerically illustrated by using two-dimensional limit-cycle oscillators as examples. As an application, we demonstrate data-driven fast entrainment with amplitude suppression using the optimal periodic input derived from the estimated phase and amplitude functions.

DOI: 10.1103/PhysRevE.106.014204

I. INTRODUCTION

There are various nonlinear rhythmic phenomena in the real world, including brain waves [1,2], animal gaits [3–6], heartbeats and respiration [7], and passive walking [8,9], many of which can be modeled mathematically as limit-cycle oscillators [10]. The phase reduction method [11–18] is useful for analyzing synchronization properties of limit-cycle oscillators subjected to weak perturbations, which represents the state of a multidimensional nonlinear oscillator using only the phase variable introduced along its limit cycle and describes the dynamics approximately by a one-dimensional phase equation. Recently, the phase reduction method has been extended to the phase-amplitude reduction method [16,19–26], which incorporates the amplitude variable characterizing the distance of the system state from the limit cycle. The resulting phase-amplitude equation can be used, for example, in deriving the optimal periodic force for stable entrainment that suppresses amplitude deviations [25,27,28].

The phase reduction method is based on the notion of the asymptotic phase [13], but it is generally not possible to analytically obtain the phase function that gives the asymptotic phase of the system state even if the explicit mathematical model of the oscillator is available. Similarly, it is not possible to analytically determine the amplitude functions of the oscillator in general. Moreover, if the mathematical model of the target oscillator is unknown, the phase and amplitude functions should be determined from observed data.

In this study, we propose a simple method for estimating the phase and amplitude functions from the time series data observed from limit-cycle oscillators without relying on their mathematical models. Rather than measuring the values of the phase and amplitude by evolving the system state until it converges to the limit cycle, we estimate them by polynomial regression from the differenced time series of the system state started from various initial conditions. Our method gives a convex optimization problem, which is computationally inexpensive and can be solved globally. We show that the phase and amplitude functions are estimated reasonably well around the limit cycle, including moderately nonlinear regimes, by the proposed method using known models of limit-cycle oscillators as examples.

For estimating the phase and amplitude functions from observed data, Extended Dynamic Mode Decomposition (EDMD) [29–31] and other system-identification methods [32–34] can also be employed. In particular, EDMD can estimate the Koopman eigenvalues and eigenfunctions of the system from observed data [30,31,35–42]. The natural frequency and Floquet exponents of the oscillator can then be

*Corresponding author: namura.n.aa@m.titech.ac.jp

evaluated from the eigenvalues, and the phase and amplitude functions can be obtained from the associated eigenfunctions [21–23,43,44]. In contrast to EDMD, our proposed method estimates the natural frequency and the dominant Floquet exponent separately from the observed data by using a conventional method for Lyapunov exponents and then uses them to estimate the phase and amplitude functions by polynomial regression. Our method thus gives an alternative to EDMD and can more robustly estimate the phase and amplitude functions depending on the data.

As closely related but different problems, methods for estimating the phase response properties of limit-cycle oscillators [6,45–51] and for estimating phase coupling functions between interacting oscillators from observed data have been proposed and applied to experimental data [1,2,52–59]. In these studies, the phase values of the oscillators are extracted from the time series, e.g., by extracting the spike timing of neural oscillators or by using the Hilbert transform, and then the phase response property of the oscillator or the phase coupling functions between the oscillators are estimated under the assumption that the oscillators are described by the phase model. The phase of the oscillator is typically estimated in the vicinity of the limit cycle and deviation from the limit cycle is not considered; unlike the present study, the phase and amplitude functions are generally not introduced explicitly.

This paper is organized as follows. We first outline the notions of asymptotic phase and amplitude in Sec. II and then describe the method for estimating the phase and amplitude functions by polynomial regression in Sec. III. The validity of the proposed method is illustrated by numerical simulations using two types of oscillators and how to evaluate the estimated results is described in Sec. IV. Section V demonstrates data-driven fast entrainment of the oscillator with amplitude suppression using the estimated phase and amplitude functions, and Sec. VI gives concluding remarks.

II. PHASE AND AMPLITUDE OF LIMIT-CYCLE OSCILLATORS

A. Asymptotic phase and amplitude functions

We first introduce the asymptotic phase and amplitude functions [19,20,22,26]. We consider a limit-cycle oscillator described by

$$\frac{d}{dt}\boldsymbol{X}(t) = \boldsymbol{F}(\boldsymbol{X}(t)), \tag{1}$$

where $\boldsymbol{X}(t) \in \mathbb{R}^N$ is the system state at time t. We assume that the system has an exponentially stable limit cycle trajectory $\boldsymbol{X}_0(t)$ with a natural period T and frequency $\omega = 2\pi/T$, which is a T-periodic function of t satisfying $\boldsymbol{X}_0(t+T) = \boldsymbol{X}_0(t)$.

First, we assign a phase $\theta \in [0, 2\pi)$ for each state on the limit cycle, where 0 and 2π are considered identical, by choosing a state $\boldsymbol{X}_0(0)$ on the limit cycle as the phase origin, $\theta = 0$, and defining the phase of the state $\boldsymbol{X}_0(t)$ at $t > 0$ as $\theta = \omega t \pmod{2\pi}$. We denote by $\boldsymbol{\mathcal{X}}_0(\theta)$ the state on the limit cycle with phase θ. Next, we extend the definition of the phase to the basin of the limit cycle. The phase of a system state $\boldsymbol{X}_A$ in the basin is defined as θ if $\lim_{t\to\infty} \|\Psi_{t,t_0}\boldsymbol{X}_A - \Psi_{t,t_0}\boldsymbol{\mathcal{X}}_0(\theta)\| = 0$ holds, where Ψ_{t,t_0} is the flow of Eq. (1) and $\|\cdot\|$ is the L_2 norm. That is, if the state $\Psi_{t,t_0}\boldsymbol{X}_A$ started from $\boldsymbol{X}_A$ at t_0 converges to the state $\Psi_{t,t_0}\boldsymbol{\mathcal{X}}_0(\theta)$ started from $\boldsymbol{\mathcal{X}}_0(\theta)$ at t_0 as $t \to \infty$, we consider that the phase state $\boldsymbol{X}_A$ has the same phase θ as $\boldsymbol{\mathcal{X}}_0(\theta)$. This defines a phase function Θ for all states $\boldsymbol{X}$ in the basin, which assigns a phase value $\theta(t) = \Theta(\boldsymbol{X}(t))$ to the state $\boldsymbol{X}(t)$ and satisfies

$$\frac{d}{dt}\theta(t) = \frac{d}{dt}\Theta(\boldsymbol{X}(t)) = \omega. \tag{2}$$

The phase defined in this way is called the asymptotic phase, and the level sets of the phase function is called "isochrons" [11–15]. The asymptotic phase can also be interpreted as the argument of the eigenfunction of the Koopman generator $\boldsymbol{F}(\boldsymbol{X})\cdot\nabla$ of Eq. (1) associated with the eigenvalue $i\omega$ [21–23,43,44].

Next, we introduce the (dominant) amplitude function. In a similar way to the phase $\theta(t)$, we assign a scalar amplitude $r(t) = R(\boldsymbol{X}(t))$ for all states $\boldsymbol{X}$ in the basin, where the amplitude function R satisfies

$$\frac{d}{dt}r(t) = \frac{d}{dt}R(\boldsymbol{X}(t)) = \lambda R(\boldsymbol{X}(t)) = \lambda r(t). \tag{3}$$

Here the coefficient $\lambda < 0$ is the Floquet exponent of the limit cycle with the largest nonzero real part, which is assumed to be real and simple. As the state $\boldsymbol{X}(t)$ converges to the limit cycle, the amplitude $r(t)$ decays exponentially and satisfies $R(\boldsymbol{\mathcal{X}}_0(\theta)) = 0$ when the state is on the limit cycle. The amplitude function can also be considered an eigenfunction of the Koopman generator $\boldsymbol{F}(\boldsymbol{X})\cdot\nabla$ of Eq. (1) associated with the eigenvalue λ. The level sets of the amplitude function is called "isostables" in the framework of the Koopman operator analysis of limit-cycling systems [21–23,43,44].

By using the phase and amplitude functions, we can reduce the dimensionality of the oscillator and globally linearize the dynamics in the basin of the limit cycle, which yields a simple description of the oscillator useful for the analysis. Moreover, near the limit cycle, we can write phase-amplitude equations describing weakly perturbed oscillatory dynamics. The simplicity of the phase equation has played a prominent role in the theoretical analysis of synchronization phenomena in various types of limit-cycling systems [11–14].

B. Response and sensitivity functions

We next introduce the response and sensitivity functions of the phase and amplitude, which are used for the validation of our estimation method.

The phase response function (PRF, also known as the phase response or resetting curve, PRC [11,13,14,60]) gives the phase difference of the oscillator caused by an impulse perturbation applied to the oscillator at phase θ and is defined as

$$\begin{aligned} g(\theta;\boldsymbol{\varsigma}) &= \Theta(\boldsymbol{\mathcal{X}}_0(\theta)+\boldsymbol{\varsigma}) - \Theta(\boldsymbol{\mathcal{X}}_0(\theta)) \\ &= \Theta(\boldsymbol{\mathcal{X}}_0(\theta)+\boldsymbol{\varsigma}) - \theta, \end{aligned} \tag{4}$$

where $\boldsymbol{\varsigma} \in \mathbb{R}^N$ represents the direction and intensity of the impulse [13–15,61,62]. When $|\boldsymbol{\varsigma}|$ is sufficiently small, we can approximate g by using the Taylor expansion of Θ near $\boldsymbol{\varsigma} = \boldsymbol{0}$, $\Theta(\boldsymbol{\mathcal{X}}_0(\theta)+\boldsymbol{\varsigma}) = \Theta(\boldsymbol{\mathcal{X}}_0(\theta)) + \nabla\Theta(\boldsymbol{X})|_{\boldsymbol{X}=\boldsymbol{\mathcal{X}}_0(\theta)}\cdot\boldsymbol{\varsigma} + O(|\boldsymbol{\varsigma}|^2)$, as $g(\theta;\boldsymbol{\varsigma}) \simeq \nabla\Theta(\boldsymbol{X})|_{\boldsymbol{X}=\boldsymbol{\mathcal{X}}_0(\theta)}\cdot\boldsymbol{\varsigma}$. We denote the

gradient of $\Theta(\boldsymbol{X})$ evaluated at the state $\boldsymbol{X} = \boldsymbol{\mathcal{X}}_0(\theta)$ by

$$\boldsymbol{Z}(\theta) = \nabla\Theta(\boldsymbol{X})|_{X=\boldsymbol{\mathcal{X}}_0(\theta)} \tag{5}$$

and call it the phase sensitivity function (PSF, also known as the infinitesimal phase resetting curve, iPRC). This $\boldsymbol{Z}(\theta)$ characterizes the linear response of the oscillator phase to a weak perturbation given at phase θ.

Similarly, we introduce the amplitude response function (ARF) characterizing the amplitude difference of the oscillator caused by an impulse $\boldsymbol{\varsigma}$ given at phase θ as

$$h(\theta;\boldsymbol{\varsigma}) = R(\boldsymbol{\mathcal{X}}_0(\theta)+\boldsymbol{\varsigma}) - R(\boldsymbol{\mathcal{X}}_0(\theta)) = R(\boldsymbol{\mathcal{X}}_0(\theta)+\boldsymbol{\varsigma}). \tag{6}$$

When $|\boldsymbol{\varsigma}|$ is sufficiently small, we can approximate h by using the Taylor expansion of $R(\boldsymbol{\mathcal{X}}_0(\theta)+\boldsymbol{\varsigma})$ near $\boldsymbol{\varsigma} = \boldsymbol{0}$, $R(\boldsymbol{\mathcal{X}}_0(\theta)+\boldsymbol{\varsigma}) = R(\boldsymbol{\mathcal{X}}_0(\theta)) + \nabla R(\boldsymbol{X})|_{X=\boldsymbol{\mathcal{X}}_0(\theta)} \cdot \boldsymbol{\varsigma} + O(|\boldsymbol{\varsigma}|^2)$, as $h(\theta;\boldsymbol{\varsigma}) \simeq \nabla R(\boldsymbol{X})|_{X=\boldsymbol{\mathcal{X}}_0(\theta)} \cdot \boldsymbol{\varsigma}$. Here we denote the gradient of the amplitude function $R(\boldsymbol{X})$ at the state $\boldsymbol{X} = \boldsymbol{\mathcal{X}}_0(\theta)$ by

$$\boldsymbol{I}(\theta) = \nabla R(\boldsymbol{X})|_{X=\boldsymbol{\mathcal{X}}_0(\theta)} \tag{7}$$

and call it the amplitude sensitivity function (ASF, also known as isostable response function in the Koopman operator analysis of limit-cycling systems). This $\boldsymbol{I}(\theta)$ characterizes the linear response of the oscillator amplitude to a weak perturbation given at θ.

If the mathematical model of the oscillator is known, the PSF $\boldsymbol{Z}(\theta)$ and ASF $\boldsymbol{I}(\theta)$ can be determined by numerically calculating the 2π-periodic solutions of the following adjoint equations [14,17,22,27,60]:

$$\omega\frac{d}{d\theta}\boldsymbol{Z}(\theta) = -\boldsymbol{J}(\theta)^\top\boldsymbol{Z}(\theta), \tag{8}$$

$$\omega\frac{d}{d\theta}\boldsymbol{I}(\theta) = -(\boldsymbol{J}(\theta)^\top - \lambda)\boldsymbol{I}(\theta), \tag{9}$$

where $\boldsymbol{J}(\theta)$ denotes the Jacobian matrix of the vector field $\boldsymbol{F}$ at $\boldsymbol{X} = \boldsymbol{\mathcal{X}}_0(\theta)$. The PSF $\boldsymbol{Z}(\theta)$ should satisfy $\boldsymbol{Z}(\theta)\cdot\boldsymbol{F}(\boldsymbol{\mathcal{X}}_0(\theta)) = \omega$ as a normalization condition. The normalization condition for the ASF can be chosen arbitrary and will be specified later.

C. Direct numerical calculation of phase and amplitude functions

It is generally difficult to obtain the phase and amplitude functions analytically from a mathematical model, but they can be obtained by direct numerical calculation of the mathematical model as follows.

For the phase function [15], we first choose a point on the limit cycle as the origin of the phase, then assign the phase values to the states on the limit cycle. For the states in the basin of the limit cycle, we let them evolve for an integer multiple of the period T until they converge to the limit cycle and then determine their phase values.

Similarly, for the amplitude function, we let the state $\boldsymbol{X}$ in the basin evolve until it becomes sufficiently close to (but not completely on) the limit cycle, and find the point $\boldsymbol{\mathcal{X}}(\theta)$ on the limit cycle with the same phase θ as $\boldsymbol{X}$. The amplitude of the point sufficiently close to the limit cycle can be obtained by taking the inner product of the vector $\Delta\boldsymbol{X} = \boldsymbol{X} - \boldsymbol{\mathcal{X}}(\theta)$ between the two points and the amplitude sensitivity function $\boldsymbol{I}(\theta)$ as $R(\boldsymbol{X}) \simeq \boldsymbol{I}(\theta)\cdot\Delta\boldsymbol{X}$, which follows from the Taylor expansion of the amplitude function.

Note that these methods are exhaustive and computationally required. We will use the phase and amplitude functions directly calculated from the mathematical model by the above method as "true" functions to characterize the accuracy of the estimated functions from the observed data.

III. PROPOSED METHOD OF ESTIMATION

A. Estimation of the frequency and Floquet exponent

In our method, the natural frequency ω and the largest nonzero Floquet exponent λ of the oscillator should be measured before the estimation of the phase and amplitude functions. The natural frequency ω can be estimated from the average period T of the system state to perform rotations. To estimate the Floquet exponents from time series data, we use the method of Wolf *et al.* [63] for the Lyapunov exponents of dynamical systems. For two-dimensional limit-cycle oscillators, the Floquet exponents are real and exactly the same as the Lyapunov exponents. As one Lyapunov exponent λ_1 corresponding to the phase direction is 0, it is enough to estimate the sum of the Lyapunov exponents, $\lambda_1 + \lambda_2$, which can be performed by measuring the evolution of a small phase-plane area for a long time. The same method can also be used for the two largest Lyapunov exponents of higher-dimensional oscillators when λ is real.

We assume that a discretized time sequence of the system state (with observation noise) from an initial condition not on the limit cycle is obtained. By taking the logarithmic ratio of the area $S(t_k)$ of the triangle formed by three nearby states in the time series at time t_k to the area $S(t_{k+1})$ at t_{k+1} and summing over a long period of time, we can obtain λ as the sum of the Lyapunov exponents:

$$\lambda = \lambda_1 + \lambda_2 = \frac{1}{t_L - t_0}\sum_{k=0}^{L-1}\ln\frac{S(t_{k+1})}{S(t_k)}, \tag{10}$$

where L is the length of the data and the area $S(t_k)$ is reset to 0.1 at each t_k so that it does not vanish due to numerical errors.

As illustrated in Figs. 1 and 6 (see Sec. IV for details), the method of Wolf *et al.* can estimate the Floquet exponents with sufficient accuracy for the observation noise assumed in this study. If the observation noise is stronger, more advanced signal processing methods suitable for individual observed signals should be employed. It is also known the method of Wolf *et al.* is not robust against strong noise [64], and various improved methods have been proposed [65–68]. We may also use those improved methods for estimating the Floquet exponents.

B. Estimation of the phase function

We first propose a method for estimating the phase function by polynomial regression from observed data of an unknown limit-cycle oscillator. We do not measure the absolute phase value of each state, which is difficult with the time series; rather, we use the phase differences between two consecutive states in the time series and use Eq. (2) for the estimation.

We assume that we can obtain discretized time sequences of $\boldsymbol{X}(t) \in \mathbb{R}^{N\times 1}$ from various initial conditions (with observation noise). Each sequence is sampled at equal intervals of Δt with M sampling points, where Δt is sufficiently smaller than the natural period T of the oscillator, namely, $\Delta t/T$ is small enough to capture the continuous oscillatory signal and its time derivative.

We construct a standardized row vector of polynomials up to order $p \geqslant 1$ from $\boldsymbol{X}$,

$$\boldsymbol{U}(\boldsymbol{X}, p) = \begin{bmatrix} 1 & \bar{x}_1 & \cdots & \bar{x}_N & \bar{x}_1^2 & \overline{x_1x_2} & \cdots & \bar{x}_N^2 & \cdots & \bar{x}_N^p \end{bmatrix} \in \mathbb{R}^{1\times P}, \tag{11}$$

where x_k is the kth component of $\boldsymbol{X}$ and all cross terms like $\overline{x_1^2x_2^3}$ up to order p are included. The overline indicates standardization, i.e., $\bar{z} =: (z-\mu)/\sigma$ is the standard score of z, where μ and σ are the mean and the standard deviation of z, respectively. We consider approximating the sine and cosine of the phase function $\Theta(\boldsymbol{X})$ by polynomials of order p as

$$\cos[\Theta(\boldsymbol{X})] \simeq \boldsymbol{U}(\boldsymbol{X}, p)\boldsymbol{z}_1, \quad \sin[\Theta(\boldsymbol{X})] \simeq \boldsymbol{U}(\boldsymbol{X}, p)\boldsymbol{z}_2, \tag{12}$$

where $\boldsymbol{z}_1 \in \mathbb{R}^{P\times 1}$ and $\boldsymbol{z}_2 \in \mathbb{R}^{P\times 1}$ are the coefficient vectors of the polynomials. Hereafter, $\boldsymbol{U}(\boldsymbol{X}, p)$ is denoted by $\boldsymbol{U}(\boldsymbol{X})$. Our aim is to find the best polynomial approximations of $\sin\Theta$ and $\cos\Theta$ that are consistent with the definition of Θ, Eq. (2), from the time series of $\boldsymbol{X}(t)$.

Taking the time derivatives of $\sin\Theta(\boldsymbol{X})$ and $\cos\Theta(\boldsymbol{X})$, we obtain

$$\begin{aligned} \frac{d}{dt}\cos[\Theta(\boldsymbol{X}(t))] &= -\omega\sin[\Theta(\boldsymbol{X}(t))], \\ \frac{d}{dt}\sin[\Theta(\boldsymbol{X}(t))] &= \omega\cos[\Theta(\boldsymbol{X}(t))], \end{aligned} \tag{13}$$

and using Eq. (12), we obtain

$$\begin{aligned} \frac{d}{dt}\boldsymbol{U}(\boldsymbol{X}(t))\boldsymbol{z}_1 &= \left[\left(\left.\frac{\partial \boldsymbol{U}(\boldsymbol{X})}{\partial \boldsymbol{X}}\right|_{\boldsymbol{X}=\boldsymbol{X}(t)}\right)^{\top}\frac{d\boldsymbol{X}(t)}{dt}\right]\cdot\boldsymbol{z}_1 \\ &\simeq -\omega\boldsymbol{U}(\boldsymbol{X}(t))\boldsymbol{z}_2, \\ \frac{d}{dt}\boldsymbol{U}(\boldsymbol{X}(t))\boldsymbol{z}_2 &= \left[\left(\left.\frac{\partial \boldsymbol{U}(\boldsymbol{X})}{\partial \boldsymbol{X}}\right|_{\boldsymbol{X}=\boldsymbol{X}(t)}\right)^{\top}\frac{d\boldsymbol{X}(t)}{dt}\right]\cdot\boldsymbol{z}_2 \\ &\simeq \omega\boldsymbol{U}(\boldsymbol{X}(t))\boldsymbol{z}_1, \end{aligned} \tag{14}$$

where $\partial\boldsymbol{U}(\boldsymbol{X})/\partial\boldsymbol{X} \in \mathbb{R}^{N\times P}$ is a matrix whose (j,k) component is given by $\partial U_k/\partial X_j$ $(j = 1,\ldots,N, k = 1,\ldots,P)$ and "$\cdot$" indicates the dot product of two vectors.

We discretize the time as $t = i\Delta t$ with a small time step Δt and represent the time series $\boldsymbol{X}(t)$ as $\boldsymbol{X}_i = \boldsymbol{X}(i\Delta t)$. We also denote numerical derivative of $\boldsymbol{X}(t)$ at $t = i\Delta t$ as $\dot{\boldsymbol{X}}_i$, which is calculated by a linear regression of several consecutive data points in the time series since observation noise is overlapped on the data [69]. From Eq. (14), the following equations should hold approximately for each $i = 1,\ldots,M$:

$$\begin{aligned} \dot{\boldsymbol{X}}_i^{\top}\left(\left.\frac{\partial \boldsymbol{U}(\boldsymbol{X})}{\partial \boldsymbol{X}}\right|_{\boldsymbol{X}=\boldsymbol{X}_i}\right)\boldsymbol{z}_1 + \omega\boldsymbol{U}(\boldsymbol{X}_i)\boldsymbol{z}_2 &= 0, \\ \dot{\boldsymbol{X}}_i^{\top}\left(\left.\frac{\partial \boldsymbol{U}(\boldsymbol{X})}{\partial \boldsymbol{X}}\right|_{\boldsymbol{X}=\boldsymbol{X}_i}\right)\boldsymbol{z}_2 - \omega\boldsymbol{U}(\boldsymbol{X}_i)\boldsymbol{z}_1 &= 0. \end{aligned} \tag{15}$$

Introducing $\boldsymbol{z} = [\boldsymbol{z}_1^{\top}, \boldsymbol{z}_2^{\top}]^{\top} \in \mathbb{R}^{2P\times 1}$, these equations can be expressed as

$$\begin{bmatrix} \dot{\boldsymbol{X}}_i^{\top}\boldsymbol{U}_i' & \omega\boldsymbol{U}_i \\ -\omega\boldsymbol{U}_i & \dot{\boldsymbol{X}}_i^{\top}\boldsymbol{U}_i' \end{bmatrix}\boldsymbol{z} =: \boldsymbol{c}_i\boldsymbol{z} = \begin{bmatrix} 0 \\ 0 \end{bmatrix}, \tag{16}$$

where $\boldsymbol{U}_i = \boldsymbol{U}(\boldsymbol{X}_i)$ and $\boldsymbol{U}'(\boldsymbol{X}_i) = \partial U(\boldsymbol{X})/\partial\boldsymbol{X}|_{\boldsymbol{X}=\boldsymbol{X}_i}$. We try to find the best coefficient vector $\boldsymbol{z}$ that satisfies the above equation as much as possible for the given time series. Defining a matrix $\boldsymbol{C}$ by $\boldsymbol{C} = [\boldsymbol{c}_1^{\top}, \boldsymbol{c}_2^{\top}, \ldots, \boldsymbol{c}_M^{\top}]^{\top} \in \mathbb{R}^{2M\times 2P}$, this gives a minimization problem of the following objective function:

$$E_{\Theta} = \|\boldsymbol{C}\boldsymbol{z}\|^2, \tag{17}$$

where $\|\boldsymbol{C}\boldsymbol{z}\|^2 = \sum_{k=1}^{2M}\{(\boldsymbol{C}\boldsymbol{z})_k\}^2$.

To fix the origin of the estimated phase function, we also require that the absolute phase of a given state $\tilde{\boldsymbol{X}}$ is zero:

$$\Theta(\tilde{\boldsymbol{X}}) = 0. \tag{18}$$

Thus, the polynomial approximations of $\cos\Theta(\tilde{\boldsymbol{X}})$ and $\sin\Theta(\tilde{\boldsymbol{X}})$ should satisfy

$$\boldsymbol{U}(\tilde{\boldsymbol{X}})\boldsymbol{z}_1 = 1, \quad \boldsymbol{U}(\tilde{\boldsymbol{X}})\boldsymbol{z}_2 = 0, \tag{19}$$

and using $\boldsymbol{z} = [\boldsymbol{z}_1^{\top}, \boldsymbol{z}_2^{\top}]^{\top}$,

$$\begin{bmatrix} \boldsymbol{U}(\tilde{\boldsymbol{X}}) & \boldsymbol{0} \\ \boldsymbol{0} & \boldsymbol{U}(\tilde{\boldsymbol{X}}) \end{bmatrix}\boldsymbol{z} = \begin{bmatrix} 1 \\ 0 \end{bmatrix}. \tag{20}$$

Considering the above objective function and the constraints, the proposed estimation method can be formulated as an optimization problem for the coefficient $\boldsymbol{z}$ as follows:

$$\begin{aligned} &\hat{\boldsymbol{z}} = \underset{\boldsymbol{z}}{\operatorname{argmin}}\ \|\boldsymbol{C}\boldsymbol{z}\|^2 \\ &\text{s.t.} \begin{bmatrix} \boldsymbol{U}(\tilde{\boldsymbol{X}}) & \boldsymbol{0} \\ \boldsymbol{0} & \boldsymbol{U}(\tilde{\boldsymbol{X}}) \end{bmatrix}\boldsymbol{z} = \begin{bmatrix} 1 \\ 0 \end{bmatrix}. \end{aligned} \tag{21}$$

This optimization problem is convex with respect to the coefficient vector $\boldsymbol{z}$.

In this study, we assume that the oscillator state is measured at a sampling rate sufficiently larger than the oscillation frequency. Therefore, the number of observed data is sufficiently larger than the number of model parameters (coefficients of the polynomials), and the estimation problem is a standard overdetermined problem. In our method, we used a simple linear regression of the consecutive data points for calculating the derivative of the observed time series, which worked well for the observation noise that we assumed (see Sec. IV). For stronger noise, estimation of the time derivative can be difficult and more sophisticated filtering methods should be employed.

C. Estimation of the amplitude function

We next develop a method for estimating the amplitude function by polynomial regression using the same observed data as in the previous subsection. For simplicity, we consider the amplitude function of a two-dimensional oscillator; the method can also be applied straightforwardly to higher-dimensional oscillators whose Floquet exponent with the largest nonzero part is real.

Since the Floquet exponents of a two-dimensional oscillator are real, i.e., a zero exponent associated with the phase (tangential) direction and another negative exponent associated with the amplitude direction, the amplitude function is also real. Therefore, we can approximate the amplitude function $R(\boldsymbol{X})$ by a polynomial as

$$R(\boldsymbol{X}) \simeq \boldsymbol{U}(\boldsymbol{X})\boldsymbol{\zeta}, \tag{22}$$

where $\boldsymbol{\zeta} \in \mathbb{R}^{P\times 1}$ is the coefficient vector. Plugging Eq. (22) into Eq. (3), we obtain

$$\left[\left(\left.\frac{\partial \boldsymbol{U}(\boldsymbol{X})}{\partial \boldsymbol{X}}\right|_{\boldsymbol{X}=\boldsymbol{X}(t)}\right)^{\top}\frac{d\boldsymbol{X}(t)}{dt}\right]\cdot\boldsymbol{\zeta} = \lambda \boldsymbol{U}(\boldsymbol{X})\boldsymbol{\zeta}. \tag{23}$$

Discretizing the time and plugging the time series data, we obtain

$$\left[\dot{\boldsymbol{X}}_i^{\top}\left(\left.\frac{\partial \boldsymbol{U}(\boldsymbol{X})}{\partial \boldsymbol{X}}\right|_{\boldsymbol{X}=\boldsymbol{X}_i}\right) - \lambda \boldsymbol{U}(\boldsymbol{X}_i)\right]\boldsymbol{\zeta} \coloneqq \boldsymbol{d}_i\boldsymbol{\zeta} = 0 \tag{24}$$

for $i = 1, \ldots, M$, where $\boldsymbol{d}_i \in \mathbb{R}^{1\times P}$. As in the case for the phase function, the numerical differentiation of $\boldsymbol{X}(t)$ is evaluated by the linear regression. Defining a matrix $\boldsymbol{D}$ by $\boldsymbol{D} = [\boldsymbol{d}_1^{\top}, \boldsymbol{d}_2^{\top}, \ldots, \boldsymbol{d}_M^{\top}]^{\top} \in \mathbb{R}^{M\times P}$, we obtain the following objective function to minimize:

$$E_R = \|\boldsymbol{D}\boldsymbol{\zeta}\|^2. \tag{25}$$

On the limit cycle, the value of the amplitude function should take 0, i.e., $R(\boldsymbol{\mathcal{X}}_0(\theta)) = 0$. This condition is given as the constraint for the polynomial approximation of R as $\boldsymbol{U}(\boldsymbol{X}_{0,i})\boldsymbol{\zeta} = 0$, where $\boldsymbol{X}_{0,i}$ $(i = 1, \ldots, M_0)$ denotes M_0 oscillator states on the limit cycle, which can be chosen at equal time intervals. Defining a matrix $\boldsymbol{U}_0$ by $\boldsymbol{U}_0 = [\boldsymbol{U}(\boldsymbol{X}_{0,1})^{\top}, \boldsymbol{U}(\boldsymbol{X}_{0,2})^{\top}, \ldots, \boldsymbol{U}(\boldsymbol{X}_{0,M_0})^{\top}]^{\top}$, we obtain

$$\boldsymbol{U}_0\boldsymbol{\zeta} = \boldsymbol{0}. \tag{26}$$

As stated previously, the scale of the amplitude can be arbitrarily chosen. To fix the scale of the amplitude function (this also fixes the scale of the amplitude sensitivity function $\boldsymbol{I}(\theta)$ introduced in Sec. II B), we specify the absolute amplitude value of a given state $\tilde{\boldsymbol{X}}$ as $R(\tilde{\boldsymbol{X}}) = r_0$ $(r_0 > 0)$ as in the case of the phase function. This point $\tilde{\boldsymbol{X}}$ should not be on the limit cycle and should be chosen near the fixed point of the system in order to capture the shape of the amplitude function appropriately. This constraint can be expressed as

$$\boldsymbol{U}(\check{\boldsymbol{X}})\boldsymbol{\zeta} \coloneqq \tilde{\boldsymbol{U}}\boldsymbol{\zeta} = r_0. \tag{27}$$

Moreover, we require that the norm of the coefficient vector $\boldsymbol{\zeta}$ does not become too large so that the estimated amplitude function does not diverge outside of the limit cycle due to the above two constraints near the fixed point and on the limit cycle. We thus include an additional objective function proportional to the norm $\|\boldsymbol{\zeta}\|^2$.

Summarizing, the proposed estimation method can be formulated as an optimization problem for the coefficient vector $\boldsymbol{\zeta}$ as follows:

$$\hat{\boldsymbol{\zeta}} = \underset{\boldsymbol{\zeta}}{\operatorname{argmin}} \|\boldsymbol{D}\boldsymbol{\zeta}\|^2 + \gamma\|\boldsymbol{\zeta}\|^2$$
$$\text{s.t.}\begin{bmatrix}\tilde{\boldsymbol{U}}\\ \boldsymbol{U}_0\end{bmatrix}\boldsymbol{\zeta} = \begin{bmatrix}r_0\\ \boldsymbol{0}\end{bmatrix}, \tag{28}$$

where γ is a parameter for the penalty for the solution norm. This optimization problem is convex with respect to the coefficient vector $\boldsymbol{\zeta}$.

The second term of the objective function in Eq. (28) takes the same form as the regularization term in the ridge regression. The hyperparameter γ was determined by using the L curve [70]. The L curve is defined by a log-log plot of the error $\|D\boldsymbol{\zeta}\|^2$ and the solution norm $\|\boldsymbol{\zeta}\|^2$. We empirically choose the value of γ where the absolute value of the slope falls below 6.

IV. VERIFICATION OF THE PROPOSED METHOD

A. Data used for estimation

In this section, we verify the validity of the proposed method by numerical simulations using two-dimensional limit-cycle oscillators, the Stuart-Landau oscillator [11,15] and the van der Pol oscillator [71–73]. The time series data are produced by numerical integration of the dynamical system from n initial states that are taken uniformly at random in a certain region, where each initial state is evolved until it converges to the limit cycle and M data points are sampled from the trajectory. Here we took n initial points to increase the number of data points outside the limit cycle, while we assumed a single time series in our explanation of the methods in Sec. III. These n time series are concatenated and treated as one time series vector, but the regression and differentiation are performed only within the individual time series.

B. Evaluation of estimated results

To examine the performance of the proposed method, we consider limit-cycle oscillators whose mathematical models are known and compare the estimated results with the true results obtained by direct numerical calculations of the mathematical models. We evaluate the estimation accuracy by comparing the PSFs, PRFs, ASFs, and ARFs obtained from the estimated and the true phase and amplitude functions. In what follows, we use normalized PRFs (nPRFs) and normalized ARFs (nARFs) defined as the PRFs and ARFs divided by the impulse intensity, respectively.

The jth component of the PSF $\boldsymbol{Z}(\theta)$ and ASF $\boldsymbol{I}(\theta)$ are obtained by numerical derivative of the estimated phase and amplitude functions as

$$\hat{Z}_j(\theta_i) = \frac{\hat{\Theta}(\boldsymbol{X}_{0,i} + \epsilon\boldsymbol{e}_j) - \hat{\Theta}(\boldsymbol{X}_{0,i} - \epsilon\boldsymbol{e}_j)}{2\epsilon} \tag{29}$$

and

$$\hat{I}_j(\theta_i) = \frac{\hat{R}(\boldsymbol{X}_{0,i} + \epsilon\boldsymbol{e}_j) - \hat{R}(\boldsymbol{X}_{0,i} - \epsilon\boldsymbol{e}_j)}{2\epsilon}, \tag{30}$$

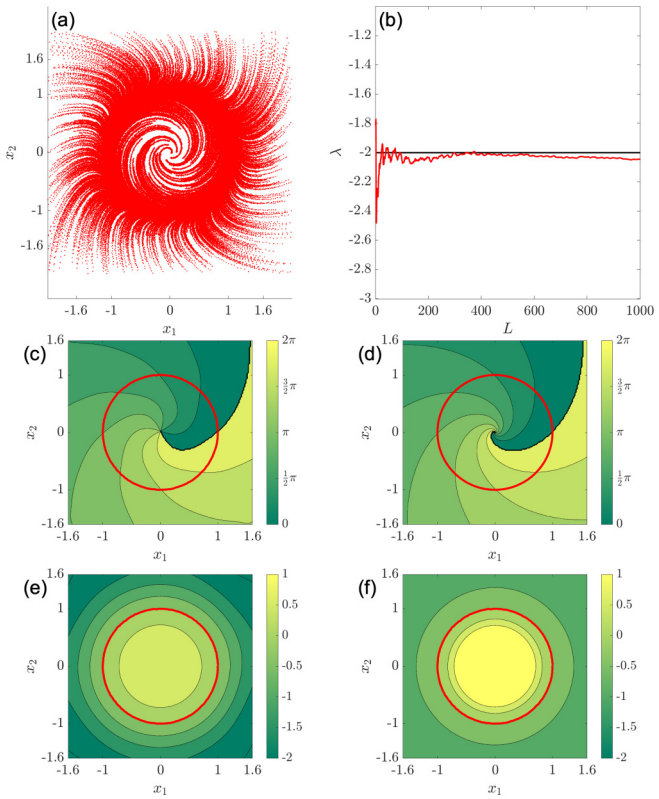

FIG. 1. Phase and amplitude functions of the SL oscillator used for the estimation. (a) Time series data used for the estimation. (b) Estimated nonzero Floquet exponent. (c) Estimated phase function. (d) True phase function. (e) Estimated amplitude function. (f) True amplitude function. In (c)–(f), the red bold circle shows the limit cycle.

for sufficiently small ϵ, where $\boldsymbol{e}_j$ is the unit vector in the jth direction and $\boldsymbol{X}_{0,i}$ is the system state on the limit cycle with phase θ_i. We use $\epsilon = 10^{-5}$ in what follows.

The nPRF $G_{\varsigma,j}(\theta) \coloneqq g(\theta, \varsigma \boldsymbol{e}_j)/\varsigma$ and the nARF $H_{\varsigma,j}(\theta) \coloneqq h(\theta, \varsigma \boldsymbol{e}_j)/\varsigma$ of the oscillator with respect to the impulse of finite intensity ς given to the jth component of the system state can be calculated from the estimated phase and amplitude functions as

$$\hat{G}_{\varsigma,j}(\theta_i) \coloneqq \frac{\hat{\Theta}(\boldsymbol{X}_{0,i} + \varsigma \boldsymbol{e}_j) - \hat{\Theta}(\boldsymbol{X}_{0,i})}{\varsigma} \tag{31}$$

and

$$\hat{H}_{\varsigma,j}(\theta_i) \coloneqq \frac{\hat{R}(\boldsymbol{X}_{0,i} + \varsigma \boldsymbol{e}_j) - \hat{R}(\boldsymbol{X}_{0,i})}{\varsigma}, \tag{32}$$

respectively.

We evaluate the accuracy of the PSFs, ASFs, nPRFs, and nARFs by using the coefficient of determination as follows:

$$R_Y^2 = 1 - \frac{\sum_i [Y_j(\theta_i) - \hat{Y}_j(\theta_i)]^2}{\sum_i [Y_j(\theta_i) - \overline{Y}_j]^2}, \tag{33}$$

where Y_j is either of Z_j, I_j, $G_{\varsigma,j}$, or $H_{\varsigma,j}$, and $\overline{Y}_j$ represents the mean of $\{Y_j(\theta_i)\}$ over i. The closer the coefficient of determination is to 1, the higher the accuracy of the estimation.

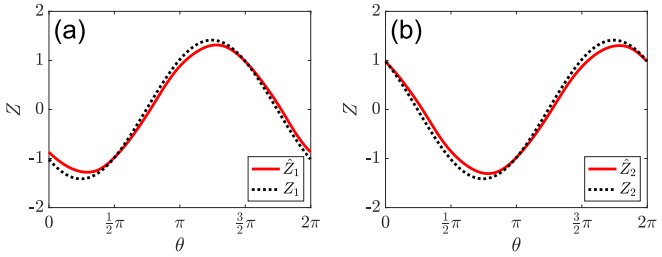

FIG. 2. Phase sensitivity functions (PSFs) of the SL oscillator. Each graph shows the estimated PSF (red solid curve) and the true PSF (black dotted curve). (a) x_1 component; (b) x_2 component. Estimated PSFs are obtained by numerical differentiation with $\epsilon = 10^{-5}$. True PSFs are calculated by solving the adjoint equation.

C. Stuart-Landau oscillator

First, we verify the validity of the proposed method using the Stuart-Landau (SL) oscillator, for which the analytical solutions of the phase and amplitude functions are obtained [74]. The SL oscillator is described as follows:

$$\frac{d}{dt}\begin{bmatrix} x_1 \\ x_2 \end{bmatrix} = \begin{bmatrix} x_1 - \alpha x_2 - (x_1 - \beta x_2)(x_1^2 + x_2^2) \\ \alpha x_1 + x_2 - (\beta x_1 + x_2)(x_1^2 + x_2^2) \end{bmatrix}, \tag{34}$$

where x_1, x_2 are the variables and $\alpha = 2$, $\beta = 1$ are parameters. We set the sampling interval as $\Delta t = 0.005$, the number of initial points as $n = 1200$, and the number of data points as $M = 500$. We estimated the phase function for the SL oscillator under the observation noise, which is given by Gaussian noise with mean 0 and standard deviation 5×10^{-3} added to the time series. The data used for the estimation are shown in Fig. 1(a). The Floquet exponents are estimated with $L = 1000$ and $t_{k+1} - t_k = 0.25$ in Eq. (10). The natural frequency is estimated as $\omega \simeq 0.9997$, and the nonzero Floquet exponent is estimated as $\lambda \simeq -2.0457$, while their theoretical values are $\omega = 1$ and $\lambda = -2$, respectively. The estimated value of the Floquet exponent is plotted with respect to the length L in Fig. 1(b). The maximum degree of the polynomial is set to $p = 18$.

We estimated the phase function Θ by the proposed method (Sec. III B) from the time series data [Fig. 1(a)]. The estimated phase function [Fig. 1(c)] is compared with the true one [Fig. 1(d)]. The phase function is accurately estimated by the proposed method except for the central and peripheral regions far from the limit cycle. The discrepancy is due to the lack of data in those regions (trajectories stay near the limit-cycle attractor most of the time) and due to the limited representation power of the polynomials.

We evaluated the estimation accuracy of the PSFs and PRFs. Figure 2 compares the PSFs Z_1 and Z_2 obtained from the estimated phase function using Eq. (29) with the true function obtained by solving the adjoint equation (8). Figure 3 compares the nPRFs $G_{\varsigma,j}$ for finite-intensity impulses obtained from the estimated phase function using Eq. (31) with the true functions obtained from the analytical solution. The estimated functions are well consistent with the true ones and the estimation error is small; the accuracy of the estimation is $R_Z^2 \geqslant 0.9859$ for the PSFs and $R_G^2 \geqslant 0.9903$ for the nPRFs, respectively (Table I). These results indicate that the proposed

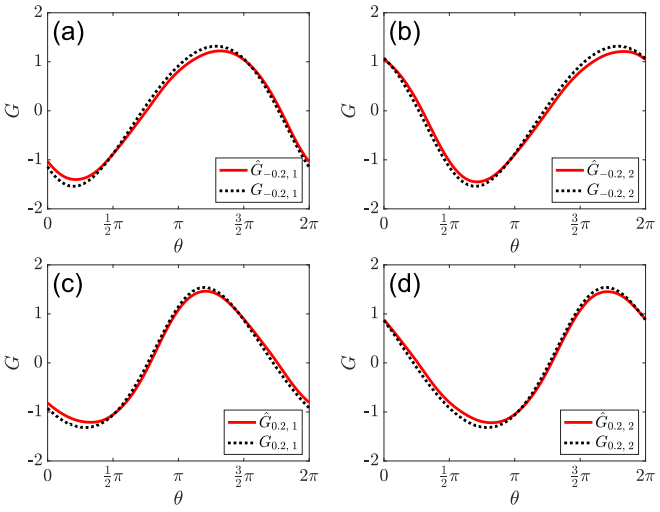

FIG. 3. Normalized phase response functions (nPRFs) of the SL oscillator. Each graph shows the estimated nPRF (red solid curve) and the true nPRF (black dotted curve). (a), (c) Impulses applied in the x_1 direction. (a) $\varsigma = -0.2$, (c) $\varsigma = +0.2$. (b), (d) Impulses applied in the x_2 direction. (b) $\varsigma = -0.2$, (d) $\varsigma = +0.2$.

method accurately estimates the phase function in the vicinity of the limit cycle and a bit farther out from the limit cycle where moderate nonlinearity comes in.

Next, we estimated the amplitude function R by the proposed method (Sec. III C) from the same time series data [Fig. 1(a)]. The hyperparameter γ is determined to be $\gamma = 1.0\times10^6$ from the L curve. The estimated amplitude function [Fig. 1(e)] is compared with the true amplitude function [Fig. 1(f)]. Our method can accurately estimate the amplitude function near the limit cycle, but the estimate deviates in the central and peripheral regions. In particular, the estimate cannot reproduce the divergence of the amplitude function near the fixed point. This discrepancy is due to the lack of data and the singularity near the fixed point of the system.

Figure 4 compares the ASFs I_1 and I_2 obtained from the estimated amplitude function using Eq. (30) with the true function obtained by solving the adjoint equation (9). Figure 5 compares the nARFs $H_{\varsigma,j}(\theta)$ obtained from the estimated amplitude function using Eq. (32) with the true results. Despite the discrepancy in the amplitude function far from the limit cycle, the estimated results agree reasonably well with the true results for the impulse intensities used here. The accuracy of estimation is $R_I^2 \geqslant 0.9998$ for the ASFs and $R_H^2 \geqslant 0.9725$ for the nARFs (Table II). These results confirm that the amplitude function is estimated appropriately around the limit cycle including moderately nonlinear regimes.

TABLE I. Coefficients of determination of the nPRFs and PSFs of the SL oscillator.

Z_1	Z_2	$G_{-0.2,1}$	$G_{-0.2,2}$	$G_{0.2,1}$	$G_{0.2,2}$
0.9869	0.9859	0.9912	0.9903	0.9927	0.9929

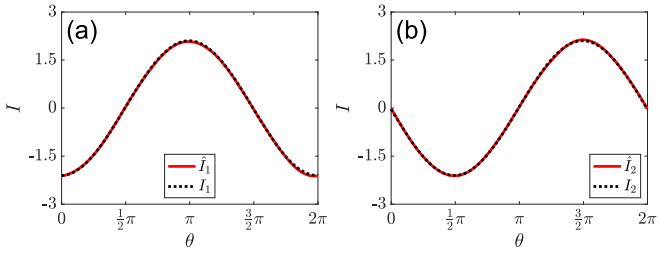

FIG. 4. Amplitude sensitivity functions (ASFs) of the SL oscillator. Each graph shows the estimated ASF (red solid curve) and the true ASF (black dotted curve). (a) x_1 component; (b) x_2 component. Estimated ASFs are obtained by numerical differentiation with $\epsilon = 10^{-5}$. True ASFs are calculated by solving the adjoint equation.

D. van der Pol oscillator

Next, we verify the validity of the proposed method using the van der Pol (vdP) oscillator. The vdP oscillator [71–73] is described as follows:

$$\frac{d}{dt}\begin{bmatrix} x_1 \\ x_2 \end{bmatrix} = \begin{bmatrix} x_2 \\ \nu(1-x_1^2)x_2 - x_1 \end{bmatrix}, \tag{35}$$

where x_1, x_2 are the variables and the parameter is chosen as $\nu = 1$. We set the sampling interval as $\Delta t = 0.005$, the number of initial points as $n = 1200$, and the number of data points as $M = 1000$. We estimated the phase function for the vdP oscillator under the observation noise, given by Gaussian noise with mean 0 and standard deviation 5×10^{-3} to the time series as the observation noise. The data used for the estimation are shown in Fig. 6(a). The Floquet exponents are estimated with $L = 1000$ and $t_{k+1} - t_k = 0.25$ in Eq. (10). The natural frequency is estimated as $\omega \simeq 0.9434$ and the nonzero Floquet exponent is estimated as $\lambda \simeq -1.0885$. The latter value agree well with the theoretical value $\lambda \simeq -1.0581$ that is evaluated from the monodromy matrix of the original model [27]. The estimated value of the Floquet exponent with

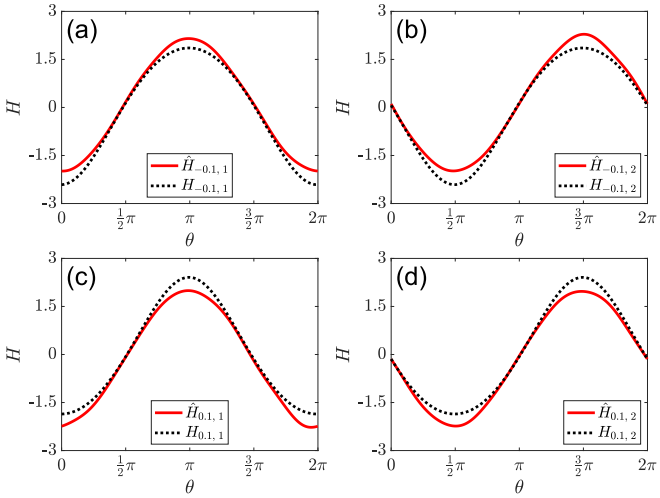

FIG. 5. Normalized amplitude response functions (nARFs) of the SL oscillator. Each graph shows the estimated nARF (red solid curve) and the true nARF (black dotted curve). (a), (c) Impulses applied in the x_1 direction. (a) $\varsigma = -0.1$, (c) $\varsigma = +0.1$. (b), (d) Impulses applied in the x_2 direction. (b) $\varsigma = -0.1$, (d) $\varsigma = +0.1$.

TABLE II. Coefficients of determination of the nARFs and ASFs of the SL oscillator.

I_1	I_2	$H_{-0.1,1}$	$H_{-0.1,2}$	$H_{0.1,1}$	$H_{0.1,2}$
0.9998	0.9999	0.9779	0.9727	0.9725	0.9742

respect to the length L is shown in Fig. 6(b). The maximum degree of the polynomial is set to $p = 18$.

We estimated the phase function Θ by the proposed method (Sec. III B) from the time series data [Fig. 6(a)]. The estimated result [Fig. 6(c)] is compared with the true phase function [Fig. 6(d)] obtained directly from the mathematical model, Eq. (35). As in the case with the SL oscillator, the estimated function is close to the true one except for the central and peripheral regions far from the limit cycle.

We examined the estimation accuracy of the PSFs and PRFs. Figure 7 compares the estimated PSFs Z_1, and Z_2 with the true ones. The estimated PSFs agree well with the true

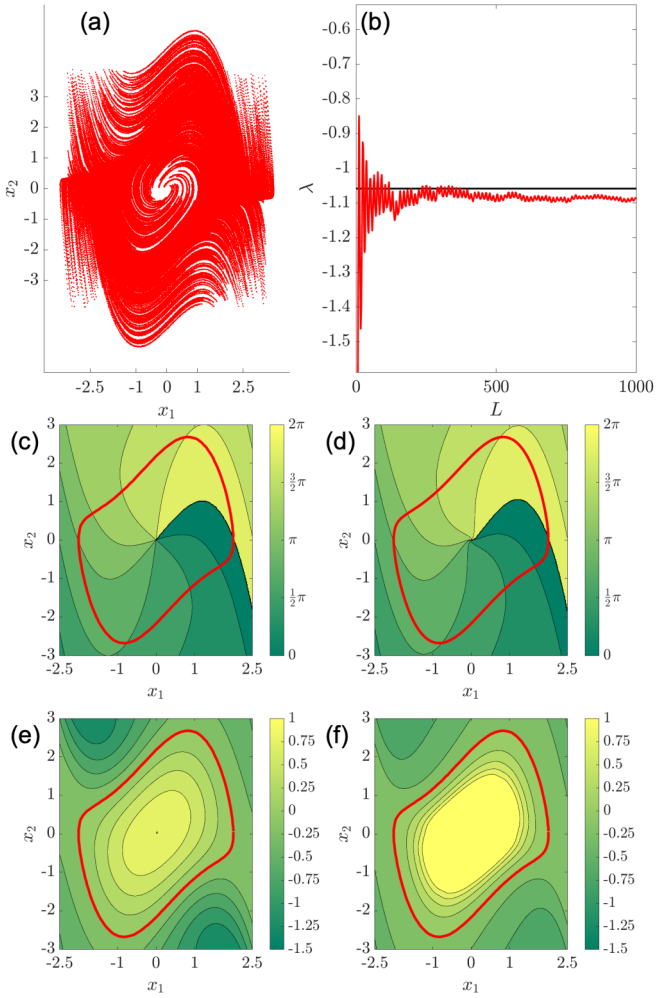

FIG. 6. Phase and amplitude functions of the vdP oscillator. (a) Time series data of the vdP oscillator used for the estimation. (b) Estimated nonzero Floquet exponent. (c) Estimated phase function. (d) True phase function. (e) Estimated amplitude function. (f) True amplitude function. In (c)–(f) the red curve shows the limit cycle.

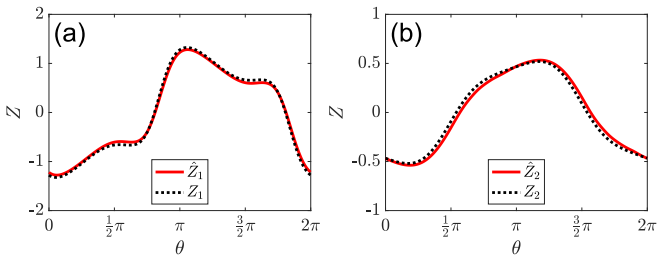

FIG. 7. Phase sensitivity functions (PSFs) of the vdP oscillator. Each graph shows the estimated PSF (red solid curve) and the true PSF (black dotted curve). (a) x_1 component; (b) x_2 component. Estimated PSFs are obtained by numerical differentiation with $\epsilon = 10^{-5}$. True PSFs are calculated by solving the adjoint equation.

PSFs, implying the accurate estimation of the phase function in the vicinity of the limit cycle. Figure 8 compares the estimated nPRFs $G_{\varsigma,j}(\theta)$ for finite-intensity impulses with the true results. Again, the estimated nPRFs agree well with the true results. Overall, the proposed method can estimate the PSFs and nPRFs accurately (Table III): $R_Z^2 \geqslant 0.9896$ and $R_G^2 \geqslant 0.9892$ for PSF and nPRFs, respectively. These results indicate that the proposed method accurately estimates the phase function in the moderately nonlinear regime around the limit cycle.

Next, we estimated the amplitude function R by the proposed method (Sec. III C) from the same data [Fig. 6(a)]. The hyperparameter γ is determined to be $\gamma = 1.0\times10^3$ from the L curve. The estimation result [Fig. 6(e)] is compared with the true amplitude function [Fig. 6(f)] obtained directly from the mathematical model, Eq. (35). As in the SL case, the estimate agrees with the true function near the limit cycle, but a discrepancy arises in the central and peripheral regions far from the limit cycle.

We examined the estimation accuracy of the ASFs and ARFs. Figure 9 compares the estimated ASFs with the true

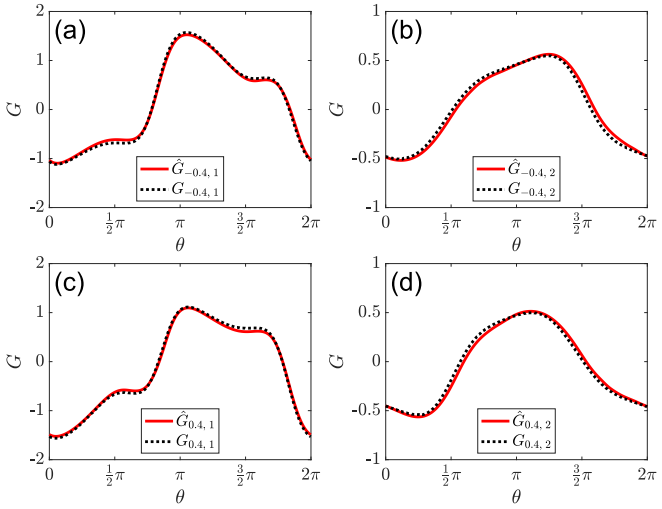

FIG. 8. Normalized phase response functions (nPRFs) of the vdP oscillator. Each graph shows the estimated nPRF (red solid curve) and the true nPRF (black dotted curve). (a), (c) Impulses applied in the x_1 direction. (a) $\varsigma = -0.4$, (c) $\varsigma = +0.4$. (b), (d) Impulses applied in the x_2 direction. (b) $\varsigma = -0.4$, (d) $\varsigma = -0.4$.

TABLE III. Coefficients of determination of the nPRFs and PSFs of the vdP oscillator.

Z_1	Z_2	$G_{-0.4,1}$	$G_{-0.4,2}$	$G_{0.4,1}$	$G_{0.4,2}$
0.9971	0.9892	0.9980	0.9896	0.9979	0.9914

ASFs, showing a reasonable agreement. Figure 10 compares the estimated nARFs with the true nARFs for finite-intensity impulses. The estimates also agree well with the true nARFs. Again, the proposed method can estimate the ASF and nARFs accurately (Table IV): $R_I^2 \geqslant 0.9792$ and $R_H^2 \geqslant 0.9694$ for ASF and nARFs, respectively. These results suggest that the proposed method estimates the amplitude function around the limit cycle accurately.

V. DATA-DRIVEN OPTIMAL ENTRAINMENT WITH AMPLITUDE SUPPRESSION

In this section we apply the proposed method to the optimal entrainment of the oscillator with amplitude suppression using the PSF and ASF developed in Ref. [27]. We consider a limit-cycle oscillator driven by an external periodic input. The natural frequency of the oscillator is ω and the frequency of the periodic input is Ω, where Ω is close to ω. When the input is sufficiently weak, the reduced and averaged phase equation for the phase difference ϕ between the oscillator and the external periodic input is given by

$$\frac{d}{dt}\phi = \Delta + \Gamma(\phi), \quad \Gamma(\phi) = [\boldsymbol{Z}(\phi + \Omega t)\cdot\boldsymbol{q}(\Omega t)]_t, \quad (36)$$

where $\Delta = \omega - \Omega$ is the frequency mismatch between the periodic input and the oscillator, Γ is the phase coupling function, $\boldsymbol{q}$ is the periodic input, and $[f(t)]_t = (\Omega/2\pi)\int_0^{2\pi/\Omega} f(s)\,ds$ denotes the average of f over one period of the external input. The optimal periodic input $\boldsymbol{q}$ can be obtained by solving the following optimization problem as discussed in Ref. [75]:

$$\boldsymbol{q} = \underset{\boldsymbol{q}}{\text{argmax}}\ -\Gamma'(\phi^*)$$
$$\text{s.t.}\quad \Delta + \Gamma(\phi^*) = 0,\ [\|\boldsymbol{q}\|^2]_t = Q, \quad (37)$$

where Γ' is the derivative of the phase coupling function at the stable phase locking point ϕ^*; the first constraint is for the system to have a phase-locked solution at ϕ^*, and the second constraint is for the power of the periodic input to be $Q > 0$. However, when the periodic input is not sufficiently weak, the trajectory deviates from the limit cycle and the above method based on the phase reduction may not work appropriately.

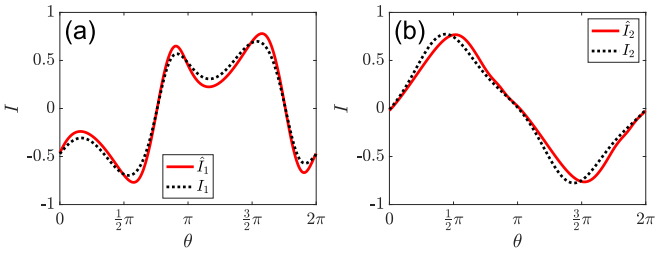

FIG. 9. Amplitude sensitivity functions (ASFs) of the vdP oscillator. Each graph shows the estimated ASF (red solid curve) and the true ASF (black dotted curve). (a) x_1 component; (b) x_2 component. Estimated ASFs are obtained by numerical differentiation with $\epsilon = 10^{-5}$. True ASFs are calculated by solving the adjoint equation.

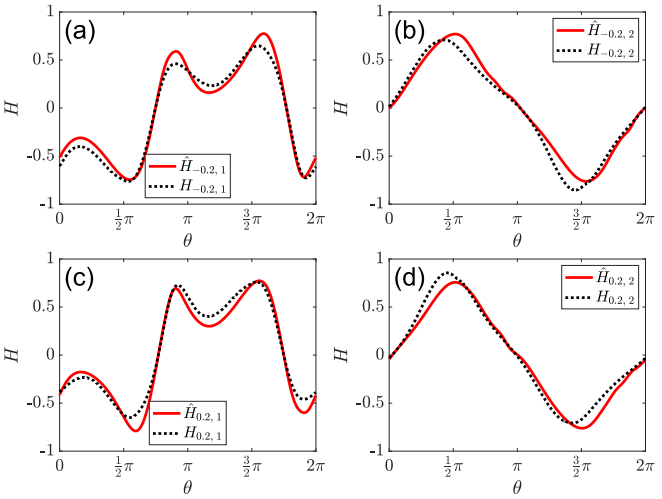

FIG. 10. Normalized amplitude response functions (nARFs) of the vdP oscillator. Each graph shows the estimated nARF (red solid curve) and the true nARF (black dotted curve). (a, c) Impulses applied in the x_1 direction. (a) $\varsigma = -0.2$, (c) $\varsigma = +0.2$. (b, d) Impulses applied in the x_2 direction. (b) $\varsigma = -0.2$, (d) $\varsigma = +0.2$.

In the amplitude-penalty method [27], the amplitude equation is also used to suppress the deviations of the trajectory from the limit cycle. It is formulated by adding a penalty term characterizing the effect of the input on the amplitude variable of the oscillator to the optimization problem (37) as follows:

$$\boldsymbol{q} = \underset{\boldsymbol{q}}{\text{argmax}}\ -\Gamma'(\phi^*) - k[\{\boldsymbol{I}(\phi^* + \Omega t)\cdot\boldsymbol{q}(\Omega t)\}^2]_t$$
$$\text{s.t.}\ \Delta + \Gamma(\phi^*) = 0,\ [\|\boldsymbol{q}\|^2]_t = Q, \quad (38)$$

where the second term in the objective function represents the penalty for the amplitude deviation and $k > 0$ is the weight of the penalty. By solving the modified optimization problem (38), the optimal input $\boldsymbol{q}$ that simultaneously improves the stability of the phase-locked solution ϕ^* and suppresses the deviation of the amplitude from the limit cycle can be obtained.

The results of the amplitude penalty method for the vdP oscillator using the PSF and ASF estimated under the observation noise are shown in Fig. 11. The parameters are set to $k = 2\times10^4$, $Q = 0.05$, $\phi^* = 0$, and $\Delta = 0$.

Figure 11(a) shows the evolution of the phase differences with and without the amplitude penalty, where results using the PSF and ASF calculated by the adjoint method (theoretical) and those estimated from the observed data (data-driven)

TABLE IV. Coefficients of determination of the nARFs and ASFs of the vdP oscillator.

I_1	I_2	$H_{-0.2,1}$	$H_{-0.2,2}$	$H_{0.2,1}$	$H_{0.2,2}$
0.9795	0.9792	0.9753	0.9694	0.9707	0.9736

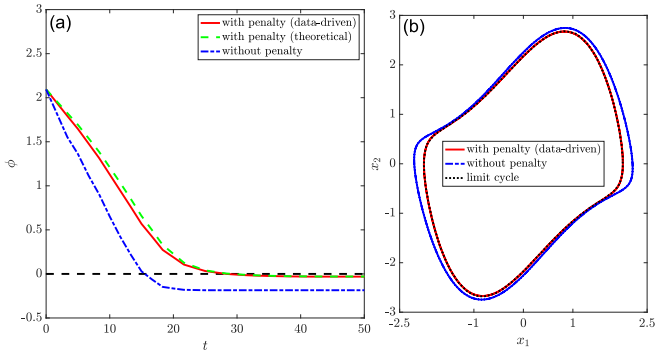

FIG. 11. Data-driven optimal entrainment of the vdP oscillator. (a) Evolution of the phase differences for the case with periodic input obtained from the estimated PSF and ASF (red solid), for the case with input obtained from true PSF and ASF (green dotted), and for the case without amplitude suppression (blue dashed). (b) Trajectories of the oscillator state; the case with periodic input obtained from the estimated PSF and ASF (red solid) and the case without the amplitude penalty (blue dashed) are compared. Black dotted curve shows the limit cycle without periodic input.

are compared. The amplitude penalty method leads to the correct phase-locking point $\phi^* = 0$, where the results using both PSFs and ASFs are almost indistinguishable, while the conventional method without amplitude suppression leads to incorrect phase-locking point different from $\phi^* = 0$ due to amplitude deviations.

Figure 11(b) shows the trajectories driven by the periodic inputs with and without amplitude penalty, where the estimated PSF and ASF are used. It can be seen that the trajectory driven by the periodic input with amplitude penalty is almost the same as the limit cycle without perturbation, while the trajectory without amplitude penalty deviates from the limit cycle. This result suggests that the proposed method is a promising approach to realize the optimal entrainment of the oscillator in a data-driven manner without the knowledge of the mathematical model.

VI. CONCLUDING REMARKS

In this study, we proposed a method for estimating the phase and amplitude functions of limit-cycle oscillators only from observed time series. Our method is based on the polynomial regression, which is simple and computationally efficient. The resulting optimization problems are convex and can be easily solved. The numerical results based on two limit-cycle oscillators (SL and vdP oscillator) showed that our method can estimate the phase and amplitude function accurately around the limit cycle under the observation noise. Furthermore, we demonstrated that the proposed method enables us to achieve the optimal entrainment with amplitude suppression in a data-driven manner, and the performance was comparable to the model-based case.

The proposed method cannot accurately estimate the phase and amplitude functions in the phase-plane regions away from the limit cycle (Figs. 1 and 6). In particular, it cannot estimate the singular behavior of the amplitude function near the fixed point of the system. However, our method accurately estimates the PSF and nPRFs (Figs. 2, 3, 7, and 8) and ASF and nARFs (Figs. 4, 5, 9, and 10) for moderate impulse intensities. In the phase-amplitude description, the PSF, nPRFs, ASF, and nARFs are essential functions for the phase-amplitude description of limit-cycle oscillators. Thus, the discrepancy of the phase and amplitude functions away from the limit cycle is not a serious problem for applications. Indeed, we demonstrated that the proposed method is useful for data-driven optimal entrainment of the limit-cycle oscillators (Fig. 11). The proposed method is potentially helpful also for data-driven analysis and control of limit-cycle oscillators subjected to pulsatile forcing or coupling [14,61,62].

As mentioned in the introduction, a major alternative to our proposed method is the EDMD [31], which estimates Koopman eigenvalues and eigenfunctions from the observed data. The asymptotic phase function Θ and amplitude function R are related to the Koopman eigenfunctions with Koopman eigenvalues $i\omega$ and λ, respectively, namely, they satisfy $(d/dt)e^{i\Theta} = i\omega e^{i\Theta}$ and $(d/dt)R = \lambda R$ [21–23,43,44].

The primary difference of the present method from those based on EDMD is that the natural frequency ω and the Floquet exponent λ are given as external parameters (measured separately) and then the phase and amplitude functions are estimated, while in the EDMD, the frequency and Floquet exponents are estimated from the time series together with the eigenfunctions.

In our simulations, EDMD often gives inaccurate values of the Floquet exponent λ as compared to the present method, which can pose a difficulty in using EDMD for estimating the reduced phase-amplitude equations from the data since the accuracy of λ is essentially important for the dynamics. The reason for this may be interpreted as follows. Since EDMD estimates the eigenvalues ($i\omega$ and λ) and the associated eigenfunctions ($e^{i\Theta}$ and R) simultaneously, estimation errors in the eigenvalues can easily be absorbed in small change in the eigenfunctions (and vice versa), leading to the difficulty in the accurate simultaneous estimation of both quantities. In contrast, our method avoids this problem by measuring ω and λ separately by using a classical robust method for the Lyapunov exponents and then estimating R and Θ. We thus think that our proposed method is complementary to the EDMD methods in the analysis of real-world oscillatory signals.

In this study, we applied the proposed method to limit-cycle oscillators with known mathematical models in order to evaluate its accuracy. Our future work is to apply the method to real-world observed data such as ECGs [7]. To this end, we plan to further develop a method of preprocessing for the time series to mitigate the effect of stronger noise and nonstationarity.

ACKNOWLEDGMENTS

H.N. acknowledges financial support from JSPS KAKENHI (Grants No. JP17H03279, No. JP18H03287, and No. JPJSBP120202201) and JST CREST (Grant No. JP-MJCR1913). R.K. thanks JSPS KAKENHI (Grants No. 18K11560, No. 19H01133, No. 21H03559, and No. 21H04571), JST PRESTO (Grant No. JPMJPR1925), and AMED (Grant No. JP21wm0525004).

[1] T. Stankovski, V. Ticcinelli, P. V. E. McClintock, and A. Stefanovska, Coupling functions in networks of oscillators, New J. Phys. **17**, 035002 (2015).

[2] T. Stankovski, V. Ticcinelli, P. V. E. McClintock, and A. Stefanovska, Neural cross-frequency coupling functions, Front. Syst. Neurosci. **11**, 33 (2017).

[3] L. Borgius, H. Nishimaru, V. Caldeira, Y. Kunugise, P. Löw, R. Reig, S. Itohara, T. Iwasato, and O. Kiehn, Spinal glutamatergic neurons defined by EphA4 signaling are essential components of normal locomotor circuits, J. Neurosci. **34**, 3841 (2014).

[4] J. J. Collins and I. N. Stewart, Coupled nonlinear oscillators and the symmetries of animal gaits, J. Nonlin. Sci. **3**, 349 (1993).

[5] R. Kobayashi, H. Nishimaru, and H. Nishijo, Estimation of excitatory and inhibitory synaptic conductance variations in motoneurons during locomotor-like rhythmic activity, Neuroscience **335**, 72 (2016).

[6] T. Funato, Y. Yamamoto, S. Aoi, T. Imai, T. Aoyagi, N. Tomita, and K. Tsuchiya, Evaluation of the phase-dependent rhythm control of human walking using phase response curves, PLoS Comput. Biol. **12**, e1004950 (2016).

[7] B. Kralemann, M. Frühwirth, A. Pikovsky, M. Rosenblum, T. Kenner, J. Schaefer, and M. Moser, *In vivo* cardiac phase response curve elucidates human respiratory heart rate variability, Nat. Commun. **4**, 2418 (2013).

[8] M. Hackel, *Humanoid Robots* (IntechOpen, Rijeka, 2007).

[9] M. Garcia, A. Chatterjee, A. Ruina, and M. Coleman, The simplest walking model: Stability, complexity, and scaling, J. Biomech. Eng. **120**, 281 (1998).

[10] S. H. Strogatz, *Nonlinear Dynamics and Chaos* (CRC Press, Boca Raton, FL, 2015).

[11] Y. Kuramoto, *Chemical Oscillations, Waves, and Turbulence* (Springer, Berlin, 1984).

[12] F. C. Hoppensteadt and E. M. Izhikevich, *Weakly Connected Neural Networks* (Springer, New York, 1997).

[13] A. T. Winfree, *The Geometry of Biological Time* (Springer, New York, 2001).

[14] G. B. Ermentrout and D. H. Terman, *Mathematical Foundations of Neuroscience* (Springer, New York, 2010).

[15] H. Nakao, Phase reduction approach to synchronisation of nonlinear oscillators, Contemp. Phys. **57**, 188 (2016).

[16] B. Monga, D. Wilson, T. Matchen, and J. Moehlis, Phase reduction and phase-based optimal control for biological systems: A tutorial, Biol. Cybern. **113**, 11 (2019).

[17] Y. Kuramoto and H. Nakao, On the concept of dynamical reduction: The case of coupled oscillators, Philos. Trans. R. Soc. A **377**, 20190041 (2019).

[18] B. Ermentrout, Y. Park, and D. Wilson, Recent advances in coupled oscillator theory, Philos. Trans. R. Soc. A **377**, 20190092 (2019).

[19] K. C. A. Wedgwood, K. K. Lin, R. Thul, and S. Coombes, Phase-amplitude descriptions of neural oscillator models, J. Math. Neurosci. **3**, 2 (2013).

[20] D. Wilson and J. Moehlis, Isostable reduction of periodic orbits, Phys. Rev. E **94**, 052213 (2016).

[21] A. Mauroy and I. Mezić, Global stability analysis using the eigenfunctions of the Koopman operator, IEEE Trans. Autom. Control **61**, 3356 (2016).

[22] S. Shirasaka, W. Kurebayashi, and H. Nakao, Phase-amplitude reduction of transient dynamics far from attractors for limit-cycling systems, Chaos **27**, 023119 (2017).

[23] A. Mauroy and I. Mezić, Global computation of phase-amplitude reduction for limit-cycle dynamics, Chaos **28**, 073108 (2018).

[24] K. Kotani, Y. Ogawa, S. Shirasaka, A. Akao, Y. Jimbo, and H. Nakao, Nonlinear phase-amplitude reduction of delay-induced oscillations, Phys. Rev. Research **2**, 033106 (2020).

[25] S. Shirasaka, W. Kurebayashi, and H. Nakao, Phase-amplitude reduction of limit cycling systems, in *Koopman Operator in Systems and Control*, edited by A. Mauroy, Alexandre, Y. Susuki, and I. Mezić (Springer International Publishing, Berlin, 2020), pp. 383–417.

[26] H. Nakao, Phase and amplitude description of complex oscillatory patterns in reaction-diffusion systems, in *Physics of Biological Oscillators: New Insights into Non-Equilibrium and Non-Autonomous Systems*, edited by A. Stefanovska and P. V. E. McClintock (Springer International Publishing, Cham, 2021), pp. 11–27.

[27] S. Takata, Y. Kato, and H. Nakao, Fast optimal entrainment of limit-cycle oscillators by strong periodic inputs via phase-amplitude reduction and Floquet theory, Chaos **31**, 093124 (2021).

[28] B. Monga and J. Moehlis, Optimal phase control of biological oscillators using augmented phase reduction, Biol. Cybern. **113**, 161 (2019).

[29] P. J. Schmid, Dynamic mode decomposition of numerical and experimental data, J. Fluid Mech. **656**, 5 (2010).

[30] J. N. Kutz, S. L. Brunton, B. W. Brunton, and J. L. Proctor, *Dynamic Mode Decomposition: Data-Driven Modeling of Complex Systems* (SIAM, Philadelphia, 2016).

[31] M. O. Williams, I. G. Kevrekidis, and C. W. Rowley, A data-driven approximation of the Koopman operator: Extending dynamic mode decomposition, J. Nonlin. Sci. **25**, 1307 (2015).

[32] B. Lusch, J. N. Kutz, and S. L. Brunton, Deep learning for universal linear embeddings of nonlinear dynamics, Nat. Commun. **9**, 4950 (2018).

[33] D. Wilson, A data-driven phase and isostable reduced modeling framework for oscillatory dynamical systems, Chaos **30**, 013121 (2020).

[34] D. Wilson, Data-driven inference of high-accuracy isostable-based dynamical models in response to external inputs, Chaos **31**, 063137 (2021).

[35] S. Klus, F. Nüske, S. Peitz, J.-H. Niemann, C. Clementi, and C. Schütte, Data-driven approximation of the Koopman generator: Model reduction, system identification, and control, Physica D **406**, 132416 (2020).

[36] Q. Li, F. Dietrich, E. M. Bollt, and I. G. Kevrekidis, Extended dynamic mode decomposition with dictionary learning: A data-driven adaptive spectral decomposition of the Koopman operator, Chaos **27**, 103111 (2017).

[37] N. Takeishi, Y. Kawahara, and T. Yairi, Learning Koopman invariant subspaces for dynamic mode decomposition, Adv. Neural Inf. Proc. Syst. **30**, 1131 (2017).

[38] D. J. Alford-Lago, C. W. Curtis, A. Ihler, and O. Issan, Deep learning enhanced dynamic mode decomposition, Chaos **32**, 033116 (2022).

[39] H. Terao, S. Shirasaka, and H. Suzuki, Extended dynamic mode decomposition with dictionary learning using neural ordinary differential equations, Nonlin. Theory Appl., IEICE **12**, 626 (2021).

[40] M. Gulina and A. Mauroy, Two methods to approximate the Koopman operator with a reservoir computer, Chaos **31**, 023116 (2021).
[41] M. O. Williams, C. W. Rowley, and I. G. Kevrekidis, A kernel-based method for data-driven Koopman spectral analysis, J. Comput. Dyn. **2**, 247 (2015).
[42] P. Héas, C. Herzet, and B. Combes, Generalized kernel-based dynamic mode decomposition, in *ICASSP 2020-2020 IEEE International Conference on Acoustics, Speech and Signal Processing (ICASSP)* (IEEE, (Virtual) Barcelona, 2020), pp. 3877–3881.
[43] A. Mauroy, I. Mezić, and Y. Susuki, *The Koopman Operator in Systems and Control: Concepts, Methodologies, and Applications*, Lecture Notes in Control and Information Sciences Vol. 484 (Springer Nature, 2020).
[44] A. Mauroy, I. Mezić, and J. Moehlis, Isostables, isochrons, and Koopman spectrum for the action-angle representation of stable fixed point dynamics, Physica D **261**, 19 (2013).
[45] R. F. Galán, G. B. Ermentrout, and N. N. Urban, Efficient Estimation of Phase-Resetting Curves in Real Neurons and its Significance for Neural-Network Modeling, Phys. Rev. Lett. **94**, 158101 (2005).
[46] K. Ota, M. Nomura, and T. Aoyagi, Weighted Spike-Triggered Average of a Fluctuating Stimulus Yielding the Phase Response Curve, Phys. Rev. Lett. **103**, 024101 (2009).
[47] T. Aonishi and K. Ota, Statistical estimation algorithm for phase response curves, J. Phys. Soc. Jpn. **75**, 114802 (2006).
[48] T. Imai, K. Ota, and T. Aoyagi, Robust measurements of phase response curves realized via multicycle weighted spike-triggered averages, J. Phys. Soc. Jpn. **86**, 024009 (2017).
[49] R. Cestnik and M. Rosenblum, Inferring the phase response curve from observation of a continuously perturbed oscillator, Sci. Rep. **8**, 13606 (2018).
[50] K. Nakae, Y. Iba, Y. Tsubo, T. Fukai, and T. Aoyagi, Bayesian estimation of phase response curves, Neural Netw. **23**, 752 (2010).
[51] K. Ota, T. Omori, S. Watanabe, H. Miyakawa, M. Okada, and T. Aonishi, Measurement of infinitesimal phase response curves from noisy real neurons, Phys. Rev. E **84**, 041902 (2011).
[52] I. T. Tokuda, S. Jain, I. Z. Kiss, and J. L. Hudson, Inferring Phase Equations from Multivariate Time Series, Phys. Rev. Lett. **99**, 064101 (2007).
[53] B. Kralemann, L. Cimponeriu, M. Rosenblum, A. Pikovsky, and R. Mrowka, Phase dynamics of coupled oscillators reconstructed from data, Phys. Rev. E **77**, 066205 (2008).
[54] A. Duggento, T. Stankovski, P. V. E. McClintock, and A. Stefanovska, Dynamical Bayesian inference of time-evolving interactions: From a pair of coupled oscillators to networks of oscillators, Phys. Rev. E **86**, 061126 (2012).
[55] T. Stankovski, T. Pereira, P. V. E. McClintock, and A. Stefanovska, Coupling functions: Universal insights into dynamical interaction mechanisms, Rev. Mod. Phys. **89**, 045001 (2017).
[56] K. Ota and T. Aoyagi, Direct extraction of phase dynamics from fluctuating rhythmic data based on a Bayesian approach, arXiv:1405.4126.
[57] T. Onojima, T. Goto, H. Mizuhara, and T. Aoyagi, A dynamical systems approach for estimating phase interactions between rhythms of different frequencies from experimental data, PLoS Comput. Biol. **14**, e1005928 (2018).
[58] K. Suzuki, T. Aoyagi, and K. Kitano, Bayesian estimation of phase dynamics based on partially sampled spikes generated by realistic model neurons, Front. Comput. Neurosci. **11**, 116 (2018).
[59] T. Arai, Y. Kawamura, and T. Aoyagi, Extracting phase coupling functions between networks of dynamical elements that exhibit collective oscillations: Direct extraction from time-series data, arXiv:2110.15598.
[60] E. Brown, J. Moehlis, and P. Holmes, On the phase reduction and response dynamics of neural oscillator populations, Neural Comput. **16**, 673 (2004).
[61] H. Nakao, K. Arai, K. Nagai, Y. Tsubo, and Y. Kuramoto, Synchrony of limit-cycle oscillators induced by random external impulses, Phys. Rev. E **72**, 026220 (2005).
[62] K. Arai and H. Nakao, Phase coherence in an ensemble of uncoupled limit-cycle oscillators receiving common poisson impulses, Phys. Rev. E **77**, 036218 (2008).
[63] A. Wolf, J. B. Swift, H. L. Swinney, and J. A. Vastano, Determining Lyapunov exponents from a time series, Physica D **16**, 285 (1985).
[64] H. Kantz and T. Schreiber, *Nonlinear Time Series Analysis* (Cambridge University Press, Cambridge, 2004).
[65] M. Sano and Y. Sawada, Measurement of the Lyapunov Spectrum from a Chaotic Time Series, Phys. Rev. Lett. **55**, 1082 (1985).
[66] J. P. Eckmann, S. O. Kamphorst, D. Ruelle, and S. Ciliberto, Liapunov exponents from time series, Phys. Rev. A **34**, 4971 (1986).
[67] R. Brown, P. Bryant, and H. D. I. Abarbanel, Computing the Lyapunov spectrum of a dynamical system from an observed time series, Phys. Rev. A **43**, 2787 (1991).
[68] U. Parlitz, Estimating Lyapunov Exponents from Time Series, in *Chaos Detection and Predictability*, edited by C. Skokos, G. Gottwald, and J. Laskar, Lecture Notes in Physics (Springer, Berlin, 2016), Vol. 915, pp. 1–34.
[69] I. Knowles and R. J. Renka, Methods for numerical differentiation of noisy data, Electron. J. Differ. Eq. **21**, 235 (2014).
[70] P. C. Hansen, Analysis of discrete ill-posed problems by means of the L-curve, SIAM Rev. **34**, 561 (1992).
[71] B. van der Pol, VII. Forced oscillations in a circuit with non-linear resistance. (Reception with reactive triode), London Edinburgh Dublin Philos. Mag. J. Sci. **3**, 65 (1927).
[72] B. van der Pol and J. van der Mark, Frequency demultiplication, Nature (London) **120**, 363 (1927).
[73] B. van der Pol, On relaxation-oscillations, London Edinburgh Dublin Philos. Mag. J. Sci. **2**, 978 (1926).
[74] Y. Kato, J. Zhu, W. Kurebayashi, and H. Nakao, Asymptotic phase and amplitude for classical and semiclassical stochastic oscillators via Koopman operator theory, Mathematics **9**, 2188 (2021).
[75] A. Zlotnik, Y. Chen, I. Z. Kiss, H.-A. Tanaka, and J.-S. Li, Optimal Waveform for Fast Entrainment of Weakly Forced Nonlinear Oscillators, Phys. Rev. Lett. **111**, 024102 (2013).